TR ADJOINT IMAGING METHOD FOR MITAT

Guoping Chen[1, 3, *], Xin Wang[1], Jinguo Wang[2], Zhiqin Zhao[2], Zaiping Nie[2], and Qinghuo Liu[3]

[1]College of Electronic & Engineering, Chongqing University of Posts and Telecommunications, Chongqing 400065, China

[2]School of Electronic Engineering, University of Electronic Science and Technology of China, Chengdu 610054, China

[3]Department of Electrical and Computer Engineering, Duke University, Durham, NC 27708, USA

Abstract—Most of the current imaging methods in microwave induced thermoacoustic tomography (MITAT) system assume that the heterogeneous sound velocity (SV) and density distribution are given or subject to Gaussian distribution. These situations generally are not satisfied. To improve multi-targets thermoacoustic sources imaging quality in a heterogeneous tissue, an iterative TR adjoint imaging method is proposed. The proposed iterative TR adjoint method can reconstruct thermoacoustic sources from the measured data even if the prior heterogeneous information of the tissue is unknown. This method estimates misfit between synthesized and observed measured signals, and iteratively updates supposed model parameters which give the heterogeneous tissue structure. In this iterative procedure, error kernels of SV, density and the approximate point source position information can be obtained independently. After the time of flight (TOF) convergence criterion is reached, a regular time reversal (TR) method with updated model will give out the final imaging result. The proposed TR adjoint imaging method is based on strictly theoretical derivation, and some simulations are presented to validate the method.

1. INTRODUCTION

The basic idea of microwave induced thermoacoustic tomography (MITAT) is that a microwave pulse heats up organ tissue with a tiny temperature change, and then the tissue generates transient thermoacoustic waves [1]. Because the electrical properties (in particular electrical conductivity) are responsible for MITAT signals, the produced MITAT image reveals the physiological and pathological status of the tissue. Many studies [2–5] have approved that tumor tissue will generate strength of thermoacoustic signals 3–7 times compared with surround normal tissue, because the tumor has high electrical properties, and fat tissue hardly generates signals. Compared to the conventional microwave and ultrasound systems, MITAT has high contrast and sensitivity for the tumor electrical conductivity, and high resolution due to the short wavelength of ultrasound wave.

The aim of an MITAT system is to image the thermoacoustic sources distribution in a biologic tissue from received ultrasound signals. However, the heterogeneity of the density and sound velocity (SV) distribution of a biological tissue have adverse effect on the imaging results. Literatures [6, 7] discovered that using an incorrect SV distribution would deteriorate both the amplitudes and the locations of the features. Different from the ultrasound or X-ray system, in which the transmitters position information is known, thermoacoustic sources information is unknown in MITAT system. Inspired from seismic study [8, 9], a method with time reversal technique and adjoint theory is proposed in this paper for the MITAT imaging. This method has some outstanding advantages: the SV and density heterogeneous information can be discovered, and the thermoacoustic sources imaging can be improved only using the received signals. In addition, the method employs full wave simulative technique to calculate the wave field, so the finite frequency characteristics of the MITAT can also be obtained.

2. PHYSICAL PRINCIPLE OF MITAT AND IMAGING INVERSE PROBLEM

Fig. 1 depicts a typical breast tumor detection measurement configuration for a two-dimensional case.

The thermoacoustic wave generated by a source will propagate through the heterogeneous medium, and it is finally received by ultrasound transducer (UT) array on the surface. The corresponding
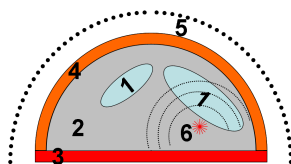
Figure 1. Schematic of the MITAT imaging problem. 1 — Heterogeneous tissue; 2 — Fat; 3 — Muscle of breast wall; 4 — Skin; 5 — Ultrasound transducers (UT) array receivers; 6 — Microwave-induced thermoacoustic source.

mathematic equations can be written as:

$$\begin{cases} \dfrac{1}{c(x)^2}\, \partial_t^2 p\,(x,t) = \rho(x)\nabla \cdot \left(\dfrac{1}{\rho(x)}\nabla p\,(x,t) \right) \ldots t \geq 0,\ x \in R^3 \\ p(x,0) = p_0(x) = f(x,t) \\ p_t(x,0) = 0 \\ p(y,t) = d(y,t),\ y \in S \times R^3 \end{cases} \quad (1)$$

where $d(y,t)$ are measured signals by transducers and y the positions of UT elements. The question that arises in Equation (1) is that generally, we do not know $c(x)$ and $\rho(x)$ before the inverse process. And the heterogeneous acoustic medium will seriously affect the imaging initial value f. So the inverse aims involved in MITAT system are the heterogeneous medium parameters $c(x)$, $\rho(x)$ and the initial value $f(x,t)$.

To solve Equation (1), many methods in terms of some special measurement configuration are developed [10–13]. Based on priori information of the heterogeneous medium parameters or the homogenous hypotheses, the phase information of the measured data can be used to reconstruct the initial value f, such as filtered back project or eigen function expansions etc. The decay at large value of time can also be used as follows: for a sufficiently large time T, one can assume that the solution is practically zero at $t = T$. Thus, imposing zero initial conditions at $t = T$ and solving in the reverse time direction, one arrives at $t = 0$ for an approximation of f. This method is named Time Reverse (TR), which was developed by the Frink etc. [14, 15]. TR method has many advantages, such as spatial-time domain filter feature and stability for medium parameters distortion. With same prior information of the heterogeneous medium, TR method can achieve the best quality among these imaging methods. In addition, TR method can also easily employ a numerical computing technique to fulfill the wave filed computation, and then reproduce the finite frequency characteristics of a MITAT signals.

However, when the heterogeneous medium parameters are unknown, the initial value f cannot be determined by above methods, i.e., the waveform or delay change in the measured data may come from the medium parameters or the initial value itself. But this analysis hints that if we predict some 'synthesized signals' at receivers using a supposed medium parameters and initial value, we can obtain the difference informations from the actual and supposed medium parameters. So we can iteratively update the supposed medium parameters and initial value until the error between the synthesized and actual observed signals reaches a proper minimum, and then we will get the best estimated model parameters. After this, a better image can be generated by a regular TR method.

3. TR ADJOINT METHOD

In Fig. 1, the heterogeneous tissue structure parameters can be denoted by $m(\rho, c)$, where ρ is the density and c the sound velocity distribution. Initial value f can be embodied as $w(t)\delta(x - x_s)$. $w(t)$ is the source's waveform, and $\delta(x - x_s)$ is its position. Our objective is to minimize a measure of the misfit between a set of data, such as waveforms or travel-times, and a complementary set of synthetics.

In order to recover the model parameters of m, we firstly suppose sources located at x_s, and their synthesized (calculated) signals at the UT transducers are $s(y, t) = \sum_{r=1}^{N} s(y_r, t)$ for a given model m. r is the UT element number and N the total element number of the UT array. If $d(y, t)$ and $s(y, t)$ are the same, m is equal to actual model, and our supposed sources are also correct. If not, we use a misfit function $F(m)$ to gauge the difference between them

$$F(m) = \frac{1}{2} \sum_{r=1}^{N} \int_{0}^{T} \|s(y_r, t) - d(y_r, t)\|^2 dt, \qquad (2)$$

where the misfit is defined by the waveform difference. Where m is current our hypothetic model parameters, and we wish to obtain an updated model $m + \delta m$ that brings us closer to a minimum of the misfit function F. We make a quadratic Taylor expansion of $F(m)$ around a particular m firstly,

$$F(m + \delta m) \approx F(m) + g(m)^T \delta m + \frac{1}{2} \delta m H(m) \delta m, \qquad (3)$$

where the gradient vector $g(m)$ is defined in terms of the first derivative

of the misfit function by

$$g(m) = \left. \frac{\partial F}{\partial m} \right|_m \quad \text{or} \ \ \delta F = g(m) \cdot \delta m. \tag{4}$$

And the Hessian matrix $H(m)$ is defined as the second derivatives of the misfit function. An updated model $m + \delta m$ may be obtained with or without the Hessian H. If the gradient and Hessian are both available, then the inverse approach is known as a Newton method; if only the gradient is available, then it is a gradient method. For complex, heterogeneous models, computation of the gradient is still feasible, but Hessian is not.

Based on Equation (4), the problem involved in our article for recovering the actual model parameters is transformed to obtain the δm. If we get it, the actual model parameters can be easily obtained by $m + \delta m$; on the other hand, Equation (4) also tells us that when there exists δm, misfit function error can be evaluated by gradient $g(m)$. If we have a particular $g(m)$ based on a given model m with δm, some optimal approximation methods can be applied to minimize δF, and we can obtain the estimated value of δm. After this procedure, we can use an updated model $m + \delta m$ to calculate a new synthesized signals $s(y, t)$, then evaluate new δF and estimate new δm until the δF reaches a proper minimum value.

Now the mathematical problem of MITAT imaging can be understood as following: we want to use Equation (2) as a criterion to obtain a δm with gradient $g(m)$ information, and the synthesized signals $s(y, t)$ are governed by Equation (1). These two parts can be combined together easily by using the scale Lagrange multiplier [16]:

$$\begin{aligned} F(m) \ = \ & \frac{1}{2} \sum_{r=1}^{N} \int_0^T \|s(y_r, t) - d(y_r, t)\|^2 dt \\ & - \int_0^T \int_\Omega \lambda \left(\frac{1}{c^2} \partial_t^2 s - \rho \nabla \cdot \left(\frac{1}{\rho} \nabla s \right) - f \right) d^3 x dt, \end{aligned} \tag{5}$$

where $\lambda(x, t)$ remains to be determined. Ω is the inter space bounded by the surface S. To facilitate mathematical treatment, we can rewrite the fist function in Equation (1) as:

$$\kappa \partial_t^2 p - \nabla \cdot (q \nabla p) - q f = 0, \tag{6}$$

where $\kappa(x) = (\rho c^2)^{-1}$, $q(x) = \rho^{-1}$, and Equation (5) can be rewritten

as:

$$F(m) = \frac{1}{2} \sum_{r=1}^{N} \int_0^T \|s(x_r,t) - d(x_r,t)\|^2 dt$$

$$- \int_0^T \int_{S \times R^3} \lambda \left(\kappa \partial_t^2 s - \nabla \cdot (q \nabla s) - qf \right) d^3x dt. \qquad (7)$$

With Lagrange multiplier, we deduce how the parameters $\kappa(x)$, $q(x)$ and $f(x,t)$ affect the misfit function. On taking the variation of Equation (7), we get:

$$\delta F = \int_0^T \int_\Omega \sum_{r=1}^N [s(y_r,t) - d(y_r,t)]\delta(x-y_r)\delta s(x,t)d^3x dt$$

$$- \int_0^T \int_\Omega \delta[\lambda \kappa \partial_t^2 s] d^3x dt + \int_0^T \int_\Omega \delta[\lambda \nabla \cdot (q\nabla p)] d^3x dt - \int_0^T \int_\Omega \delta[\lambda(qf)] d^3x dt. (8)$$

After simple algebra, we arrive at:

$$\delta F = - \int_0^T \int_\Omega dt d^3x [\delta\kappa \left(\lambda \partial_t^2 s \right) - \delta q(\nabla\lambda \cdot \nabla s) - \delta(qf)\lambda]$$

$$+ \int_0^T \int_\Omega \sum_{r=1}^N [s(x,t) - d(x,t)]\delta(x-x_r)\delta s(x,t)d^3x dt$$

$$- \int_0^T \int_\Omega dt d^3x \left[\kappa \partial_t^2 \lambda - \nabla \cdot (q\nabla\lambda) \right] \delta s - \int_\Omega d^3x \left[\kappa(\lambda \cdot \partial_t - \partial_t\lambda)\delta s \big|_0^T \right]$$

$$- \int_0^T \int_{\partial\Omega} dt d^3x \left[\hat{n} \cdot (q\nabla\lambda)\delta s \right] \qquad (9)$$

When there were no perturbations in the model parameters $\kappa(x)$, $q(x)$ and $f(x,t)$, the variation in Equation (9) is stationary with respect to perturbations δs provided that the Lagrange multiplier λ satisfies the equation

$$\kappa \partial_t^2 \lambda - \nabla \cdot (q\nabla\lambda) = \sum_{r=1}^N [s(y_r,t) - d(y_r,t)]\delta(x-y_r). \qquad (10)$$

Subject the free surface boundary condition and the end conditions

$$\hat{n} \cdot (q\nabla\lambda) = 0 \text{ on } \partial\Omega, \quad \lambda(x,T) = 0, \quad \partial_t\lambda(x,T) = 0, \qquad (11)$$

to Equation (9), meanwhile employ the nature of the Lagrange multiplier wave field, define the adjoint wave field in terms of the Lagrange multiplier wave field as

$$\lambda \equiv s^+(x,t) = s(x,T-t) - d(x,T-t), \qquad (12)$$

Equation (9) reduces to

$$\delta F = -\int_0^T \int_\Omega dt d^3x \left[\delta\kappa \left(s^+ \partial_t^2 s \right) - \delta q \left(\nabla s^+ \cdot \nabla s \right) - \delta(qf)s^+ \right]. \quad (13a)$$

Moreover, we use the initial value to define $f = w(t)\delta(x - x_s)$, and Equation (13a) can be rewritten as

$$\delta F = \int_\Omega d^3x [\delta\kappa k_\kappa + \delta q k_q + \delta(x_s)k_s]$$

$$k_\kappa = -\int_0^T dt(s^+ \partial_t^2 s)$$

$$k_q = \int_0^T dt[(\nabla s^+ \cdot \nabla s) + w(t_s)\delta(x - x_s)] \qquad . \qquad (13b)$$

$$k_s = \int_0^T dt[w(t_s)\nabla s^+(x_s)]$$

Here K_q means the sensitivity to m's q error, and we name it q kernel. K_κ means the κ sensitivity kernel, and k_s is the sensitivity kernel to the given source position. As in MITAT system, all sources are irradiated at the same time, so the waveform item $w(t_s)$ is not variable. Because s^+ comes from the perturbation sources, it must be adjoint with a synthesized procedure, so it is named as adjoint wave field. Equation (13b) means that we can calculate the sensitivity kernel based on a given model m through interacting between the adjoint wave field s^+ and synthesized wave field s, and they are embodiment of $g(m)$. After this, the model m and source position can be iteratively updated to achieve the actual values.

4. NUMERICAL IMPLEMENTATION AND SIMULATIVE RESULTS

From the kernel expressions (13b), it is obvious that to perform the time integration, simultaneous access to the synthesized wave field s at time t and the adjoint wave field s^+ at time $T - t$ are required.

4.1. Numerical Implementation

To avoid the storage for all the time steps of both s and s^+, we can employ the TR method to obtain the interaction between $s(x, t)$ and $s^+(x, T - t)$ in a unique time step. Observed that in a time invariable medium, TR method can reproduce wave field at $T - t$ time step, this procedure can be fulfilled by imposing time reversed received signals as
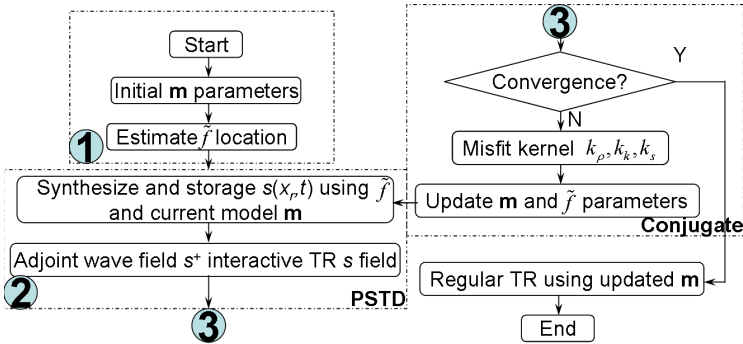
the initial condition and locating these signals at the receiver. Fig. 2 is an implementation flowchart of our proposed TR adjoint method.

There are still four problems involved in our TR adjoint numerical implementation, and they should be considered. The first problem is that in Equation (13b), if we want to get K_κ kernel, at least three time steps wave filed should be stored for the calculation of second order time derivative of synthesized wave field, which will increase the storage burden. To decrease the storage burden, we can take Equation (6) into consideration again. For wave field, the govern equation is $\partial_t^2 p = \kappa \nabla \cdot (\frac{1}{\rho} \nabla p)$, which means that the second order time derivative of the pressure wave field can be calculated by $\kappa \nabla \cdot (\frac{1}{\rho} \nabla p)$, so the second function in Equation (13b) can be rewritten as:
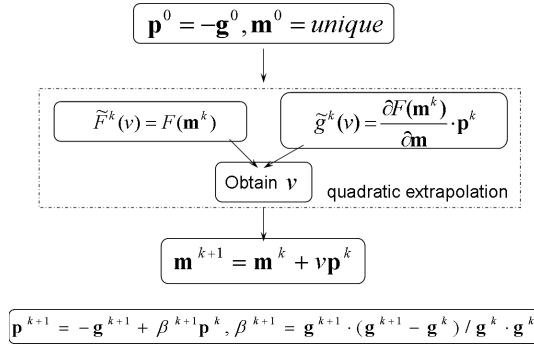
$$k_\kappa = -\int_0^T dt \left[\kappa s^+ \nabla \cdot (q \nabla s) \right].$$ (14)

Using Equation (14), we only calculate the spatial derivative of the synthesized wave field two times at one time step, and the wave field at different time steps is not necessary to storage any more.

The second problem is how to obtain the sound velocity kernel K_c from the K_κ kernel. In Equation (1), the model parameter is defined by ρ and c, not κ, q. To get K_c, one way is to calculate the K_q firstly and update the density parameter, then get the sound velocity misfit kernel K_c from K_κ. As mentioned that the received signals are pressure p, there exists $p = \rho c^2$. When there are same perturbations for ρ and c, the latter has more numerical effect on p. In a realistic consideration, such as the tumor detection in breast model, there only exist 10% perturbations for them, so the density perturbations can be neglected in general case. Based on the assumption and definition of

(a)

$$\boxed{\mathbf{p}^0 = -\mathbf{g}^0, \mathbf{m}^0 = unique}$$

$$\boxed{\widetilde{F}^k(v) = F(\mathbf{m}^k)} \qquad \boxed{\widetilde{g}^k(v) = \frac{\partial F(\mathbf{m}^k)}{\partial \mathbf{m}} \cdot \mathbf{p}^k}$$

$$\boxed{\text{Obtain } v} \quad \text{quadratic extrapolation}$$

$$\boxed{\mathbf{m}^{k+1} = \mathbf{m}^k + v\mathbf{p}^k}$$

$$\boxed{\mathbf{p}^{k+1} = -\mathbf{g}^{k+1} + \beta^{k+1}\mathbf{p}^k, \beta^{k+1} = \mathbf{g}^{k+1} \cdot (\mathbf{g}^{k+1} - \mathbf{g}^k)/\mathbf{g}^k \cdot \mathbf{g}^k}$$

(b)

Figure 2. TR adjoint method flowchart and conjugate gradient framework. There are three major parts in our flowchart. The first is initial m parameters setup and sources location estimation. Generally, the initial m parameters ρ and c are set to a homogenous value. These sources location estimation can employ once TR or back-projection method with the observed signals and initial m parameters, then pick the maximum value as f. In the second part, $s(y, t)$ are synthesized and stored based on current model and f, then adjoint wave filed s^+ interacts with s, s^+ using forward simulation with adjoint sources defined by Equation (12), s using TR method to obtain the $T - t$ time step wave field. All the wave field simulations in the second part use pseudo-spectrum time domain (PSTD) numerical technique. After the second part, whether the synthesized signals converge to the observed signals should be judged. We use time of fight (TOF) to evaluate the error between them. If the synthesized signals do not converge to the observed signals, the misfit kernels should be calculated based on Equation (13b). When we have these kernels, current model m and source f location can be updated based on conjugate gradient method, then new m and f can be taken into part 2 again. When the convergence criterion is reached, a regular TR method is employed to image the observed signals using an updated m model. (a) TR adjoint method flowchart. (b) Conjugate framework.

$\kappa(x) = (\rho c^2)^{-1}$, we have

$$\delta\kappa = \delta\left(1/\rho c^2\right) \approx -2\rho^{-1}c^{-2}\delta\ln c, \tag{15}$$

where $\delta\ln c = \delta c/c$, and it is the sound velocity perturbation to the given value. Substituting Equations (14) and (15) into Equation (13a),

we get the final equation:

$$\delta F = \int_{\Omega} d^3x [\delta \ln c k_{\ln c} + \delta \rho k_{\rho} + \delta(x_s) k_s]$$

$$k_{\ln c} = \int_0^T dt (s^+ \partial_t^2 s) 2 / \rho c^2 = \int_0^T dt \left(2s^+ \nabla \cdot \left(\frac{1}{\rho} \nabla s \right) \right)$$

$$k_{\rho} = \int_0^T dt [(\nabla s^+ \cdot \nabla s) + h(t_s)\delta(x - x_s)]^{-1} \tag{16}$$

$$k_s = \int_0^T dt [h(t_s) \nabla s^+(x_s)]$$

where $k_{\ln c}$ is SV sensitivity kernel to the given value (current SV), so it is a relative value.

The third problem is what numerical method should be used to implement the wave-field computing. For MITAT signal has a bandwidth of 0.5–1000.0 kHz [17], time domain method has more advantages, and pseudo-spectrum time domain method [18] is a good choice. In PSTD, the time and spatial derivatives of Equation (1) are transformed to the spectrum domain, and effectively calculated by the (Inverse) fast Fourier transfer ((I)FFT).

The last problem is about the iterative and conjugate gradient strategy. We use Fig. 2(b) as our conjugate gradient strategy. After we have the misfit kernels, where we suppose that v and $F^k(\mathbf{m} + v\mathbf{p}^k)$ are quadratic relationship, with which we want to predict the v which makes $F^k(\mathbf{m} + v\mathbf{p}^k)$ become zero using a known $v = 0$, $F^k(\mathbf{m}^k)$ value. So v can be determined by:

$$v = -2F^k \left(\mathbf{m}^k \right) \Big|_{v=0} / \tilde{g}^k \left(\mathbf{m}^k \right) \Big|_{v=0}. \tag{17}$$

where $\tilde{g}^k(\mathbf{m}^k)$ is the scale edition of $g^k(\mathbf{m}^k)$, $\tilde{g}^k(\mathbf{m}^k) = \frac{\partial F(\mathbf{m}^k + v\mathbf{p}^k)}{\partial \mathbf{m}} \cdot \mathbf{p}^k$. Conjugate gradient search vector $\mathbf{p}$ can be obtained by:

$$\mathbf{p}^{k+1} = -\mathbf{g}^{k+1} + \beta^{k+1} \mathbf{p}^k, \quad \beta^{k+1} = \mathbf{g}^{k+1} \cdot \left(\mathbf{g}^{k+1} - \mathbf{g}^k \right) / \mathbf{g}^k \cdot \mathbf{g}^k, \tag{18}$$

In our conjugate gradient iterative process, $F^k(\mathbf{m}^k)$ is normalized to one receiver and $\tilde{g}^k(\mathbf{m}^k)$ normalized to one pixel. And time of fight (TOF) is used as convergence criterion, which is the time value index the maximum amplitude value of the signal.

4.2. Simulation Model Configuration and Regular TR Method Results

In Fig. 3, we first illustrate the model parameters depending feature of the regular TR method.

As shown in Fig. 3(b), we cannot get a perfect focus image for the actual 7 point sources, because the SV parameter is set as homogenous 1650 m/s, i.e., there is 10% perturbation from the actual maximum SV value.

4.3. Multi Sources TR-adjoint Result

Also we use Fig. 3(a) model and depict the backward s, forward wave field s^+, then calculate the $k_{\ln c}$ kernel by given 7 point sources irradiating a homogenous 1500 m/s SV model. The density and source position error current have not been considered yet.

Figure 4 depicts the final $k_{\ln c}$ and corresponding SV modified model at the second iterative procedure depicted by Fig. 2(a).

The SV modified model based on Fig. 4(a) $k_{\ln c}$ kernel is depicted in Fig. 4(b). It comes from the Fig. 4(a), which is a relative SV misfit kernel, so the absolute error is $k_{\ln c}\mathbf{m}$, where $\mathbf{m}$ is current SV value, and then updated SV can be obtained by Fig. 2(b) strategy. The maximum

(a)   (b)
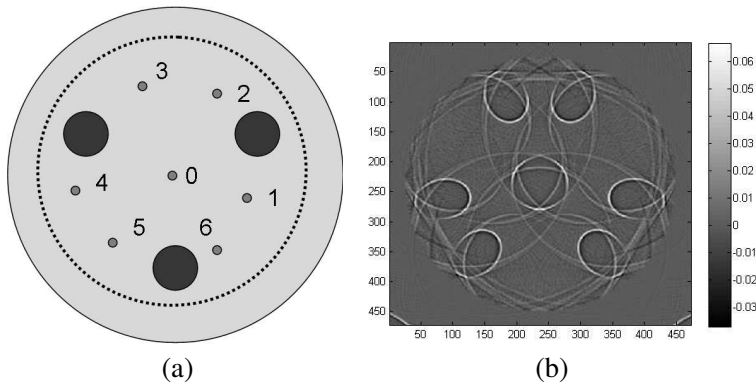
Figure 3. Actual model parameters and the parameters dependence feature of the regular TR method. (a) Model, sources and UT array. Three 18 mm radii and SV 1800 m/s heterogeneous medium areas (dark circles) are symmetrically located at a 65 mm radius circle. The 512 elements UT array (dotted circle) are evenly located at a 90 mm radius circle. Six point sources (gray points) are located symmetrically on a 65 mm radius circle, and another is located at the center, the angle between the two sources is 40 degree. All the sources have normalized strength, Gaussian waveform. The total pixels are 472×472, and extern 20 pixels PML surround the model. A 200×200 mm biological tissue is discretized by this model. (b) Regular TR method to image all 7 sources using a homogenous 1650 m/s SV model parameter estimation.
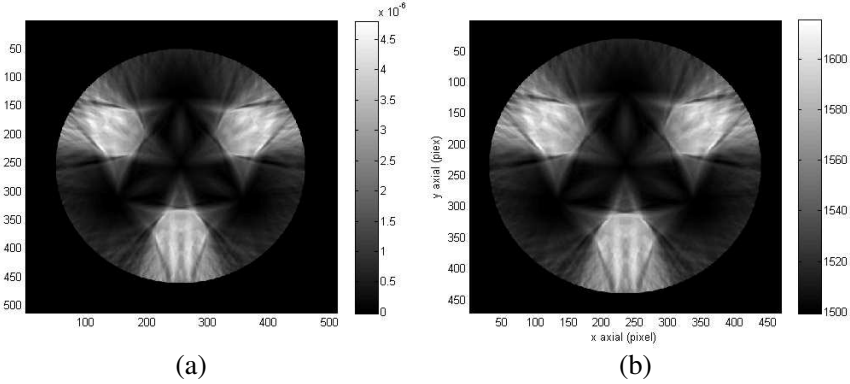
Figure 4. (a) $k_{\ln c}$ kernel and (b) the SV modified model.

value in Fig. 4(b) is 1615 m/s. In Figs. 4(a) and (b), we can get the approximate circle form appearance, which can attribute to the more than one source irradiating. If there is only one source irradiating, we can only get 3 section areas. Because 7 sources are used, we can obtain more information about the heterogeneous areas. Obviously, more source irradiating there is, more details about the heterogeneous areas we can get. Additional, because the SV modified model linearly comes from the $k_{\ln c}$ kernel, Figs. 4(a) and (b) have same appearance.

4.4. Iterative and Optimization

By now, we can get the $k_{\ln c}$ kernel and use it to get the updated SV model. Next, we give the iterative result based on the Fig. 2 flowchart.

  After 3 iterative procedures, the maximum value of $k_{\ln c}$ kernel decreases slightly from 4.85×10^{-6} to 2.2×10^{-6}, and the circle form appearances for these irradiating sources are the same. The maximum value of SV modified model is 1770.8 m/s, which is very close to the actual value 1800 m/s. To depict the result after 3 iterative processes, Fig. 5 gives the TOF comparison between the observed signals and synthesizes signals for source 0.

  In our simulation, the TOF average square error (ASE) is used as the converge criterion, and the time point index the maximum value of each synthesized signal of the receiver is recorded. TOFs are gray solid, green dashed, and red solid lines depicted in Fig. 5(a), and the observed signal's TOF is depicted as blue dot lines. Normalized ASE is defined as the average value of all 512 received signals, which means normalized ASE= $\frac{1}{N} \sum\limits_{r=1}^{N} \left(s_{\text{TOF}}(y_r) - d_{\text{TOF}}(y_r) \right)^2$. Based on this

definition, normalized ASE at iteration 0 is 9.10E-10; iteration 1 is 6.48E-11; iteration 2 is 4.4E-11. And then we depict the imaging result generated by a regular TR method with updated model m in Fig. 5(b). To compare the focus feature with and without using our proposed TR adjoint method for all the point sources, 3 spatial pressure values extracted from Fig. 3(b), Fig. 5(b), and original source pressure are plotted in Fig. 5(c). In other words, center row data in Fig. 3(b) and Fig. 5(b) are picked out. In Fig. 5(c), the black dotted line is the original source pressure waveform; the blue dashed line is imaging result wave form without using the updated SV parameter; red solid line is imaging result wave form with using the updated SV parameter. Comparing the blue dashed and red solid lines, the latter is more close to the original pressure wave form. It is shown from Fig. 5(b) that the


(a)

(b)

(c)
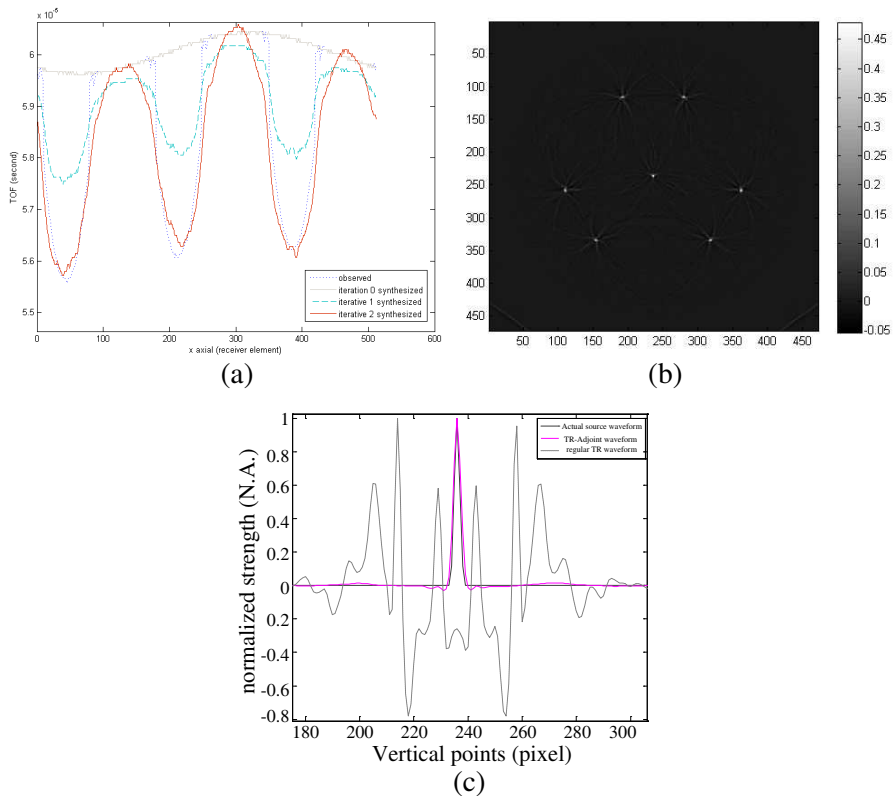
Figure 5. Converge determined by the TOF. (a) TOFs of signals. (b) TR imaging with updated SV model. (c) Spatial pressure waveform compare.

blue dashed line has many vibrations, because the incorrect SV model cannot make all the observed reversed signals with in-phase focus to a point. The red solid line depicted in Fig. 5(b) shows that the imaging result has very good focus feature.

4.5. Source Positioning

Except that the SV model updating can be obtained by using the TR adjoint method, the source location error can also be obtained, which means that in general, the supposed irradiating sources used in the TR adjoint method are imprecise, and we can estimate the error between the supposed and correct source locations by the fourth function in Equation (16). Fig. 6 depicts source 0 placed at 5 supposed locations and calculated k_s values.

Departure (pixel)	20	10	-10	-20	-30
Ks (E-5)	1.779	1.18	-1.177	-1.794	-2.027

(a)   (b)
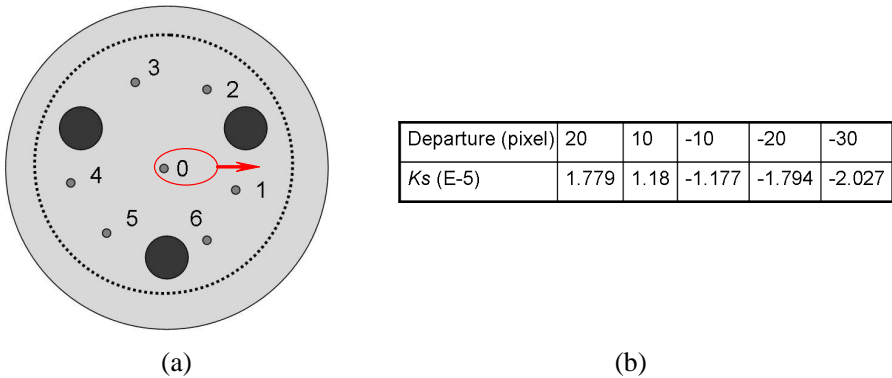
Figure 6. Source positioning error estimation. (a) Test model. (b) Calculated K_s kernel.

In Fig. 6, we move the center source along the horizon direction. Each time the supposed source moves 10 pixels from the left to the right, and the synthesized signals are generated by this source in an actual SV model. The corresponding K_s kernel is depicted in Fig. 6(b). It can be seen from Fig. 6(b) that the K_s kernel indexes the supposed source departure from the correct position.

5. DISCUSSION AND CONCLUSIONS

By now, we present the proposed original TR adjoint method for MITAT imaging thermoacoustic sources, and many things need to be considered again. The first thing is about the irradiating sources' number. Only, at most, 7 sources are used in our article, as shown

in Fig. 4(b). More heterogeneous details can be obtained using more sources, and better imaging results can be expected by a final updated model. The second thing is about the computing efficiency. As depicted in Fig. 2(a), in an iterative cycle, there are 2 computing processes for all sources, and the time consumption of each PSTD computing is about 18 minutes fulfilled by a matlab R7.2 edition codes in a server computer with eight 2.4 GHz CPUs, 48G Byte memories, 64 bit windows 7 operation system. Our codes use only one CPU resource. The total time-consumption of 3 iterations for 7 sources is about 48 minutes, and the memory usage is about 700 MByte, which depends on the simulative scale. The advantage of our numerical implementation is that the time-consumption depends only on the simulative scale, and the finite frequency information of the MITAT signals can be accurately reproduced. Based on the computing efficiency, in our article, only 3 iterative results are presented. After the last iteration, the normalized ASE of the TOF is 4.4E-11, which means that average absolute error of each TOF at one receiver is 0.29 μs. If the SV of MITAT signal is 1500 m/s, it is about 0.45 mm error in spatial. The total scale is 200×200 mm, which is discretized in 512×512 pixels, so scale of each pixel is about 0.39 mm, i.e., the 0.45 mm spatial error is about 1.15 pixels. We think that it has reached a good iterative convergence condition.

Another simulative case with maximum SV perturbation 33% model has also been tested. In this test, the maximum SV is 2000 m/s, and the background is still 1500 m/s. The results validate the proposed method.

The proposed TR adjoint method for the MITAT thermoacoustic sources imaging has many outstanding advantages. First of all, better imaging result generated by a regular TR method with updated model can be expected. Secondly, the heterogeneous details can be obtained at the same time. In some medical imaging application, these details are as important as thermoacoustic targets. Thirdly, the sources position estimation can also be improved by the proposed method. In addition, the SV information and source position estimation only come from the observed received signals.

REFERENCES

1. Chen, G. P., Z. Q. Zhao, Z. P. Nie, and Q. H. Liu, "A computational study of time reversal mirror technique for microwave-induced thermo-acoustic tomography," *Journal of Electromagnetic Waves and Applications*, Vol. 22, No. 12, 2191–2204, 2008.

2. Guo, B., Y. Wang, J. Li, P. Stoica, and R. Wu, "Microwave imaging via adaptive beamforming methods for breast cancer detection," *Journal of Electromagnetic Waves and Applications*, Vol. 20, No. 1, 53–63, 2006.

3. Catapano, I., L. Di Donato, L. Crocco, O. M. Bucci, A. F. Morabito, T. Isernia, and R. Massa, "On quantitative microwave tomography of female breast," *Progress In Electromagnetics Research*, Vol. 97, 75–93, 2009.

4. Chen, G., Z. Zhao, W. Gong, Z. Nie, and Q. Liu, "The development of the microwave-induced thermo-acoustic tomography prototype system," *Chinese Science Bulletin*, Vol. 52, No. 12, 1786–1789, 2009.

5. Kruger, R. A., W. L. Kiser, D. R. Reinecke, G. A. Kruger, and R. L. Eisenhart, "Thermoacoustic computed tomography of the breast at 434 MHz," *IEEE MIT-S Digest*, Vol. 2, 591–595, 1999.

6. Hristova, Y., P. Kuchment, and L. Nguyen, "Reconstruction and time reversal in thermoacoustic tomography in acoustically homogeneous and inhomogeneous media," *Inverse Problems*, Vol. 24, No. 5, 055006–055032, 2008.

7. Treeby, B. E., J. G. Laufer, E. Z. Zhang, F. C. Norrisy, M. F. Lythgoey, P. C. Beard, and B. T. Cox, "Acoustic attenuation compensation in photoacoustic tomography: Application to high-resolution 3D imaging of vascular networks in mice," *Photons Plus Ultrasound: Imaging and Sensing*, edited by Alexander A. Oraevsky, Lihong V. Wang, *Proc. of SPIE*, Vol. 7899, 78992Y-1-9, 2011.

8. Tape, C., Q. Liu, and J. Tromp, "Finite-frequency tomography using adjoint methods — Methodology and examples using membrane surface waves," *Geophysical Journal International*, Vol. 168, 1105–1129, 2007.

9. Norton, S. J., "Iterative inverse scattering algorithms: methods of computing Frechet derivatives," *The Journal of the Acoustical Society of America*, Vol. 106, No. 5, 2653–2660, 1999.

10. Kunyansky, L., "Fast reconstruction algorithms for the thermoacoustic tomography in certain domains with cylindrical or spher-

ical symmetries," *Inverse Problems and Imaging*, Vol. 6, No. 1, 111–131, 2011.

11. Qian, J., P. Stefanov, G. Uhlmann, and H. Zhao, "An efficient Neumann-series based algorithm for thermoacoustic and photoacoustic tomography with variable sound speed," *SIAM Journal on Imaging Sciences*, Vol. 4, No. 3, 850–883, 2011.

12. Zhang, Z. and W. Dou, "A compact THz scanning imaging system based on improved reverse-microscope system," *Journal of Electromagnetic Waves and Applications*, Vol. 24, No. 8, 1045–1057, 2010.

13. Wang, J., Z. Zhao, J. Song, X. Zhu, Z.-P. Nie, and Q. H. Liu, "Reconstruction of microwave absorption properties in heterogeneous tissue for microwave-induced thermo-acoustic tomography, *Progress In Electromagnetics Research*, Vol. 130, 225–240, 2012.

14. Fink, M., "Time-reversed acoustics," *Physics Today*, Vol. 50, No. 3, 34–40, 1997.

15. Bal, G. and L. Ryzhik, "Time reversal and refocusing in random environment," *SIAM Appl. Math.*, Vol. 63, 1375–1498, 2003.

16. Everett, H. I. I. I., "Generalized lagrange multiplier method for solving problems of optimum allocation of resources," *Operations Research*, Vol. 11, No. 3, 399–417, 1963.

17. Chen, G.-P., W.-B. Yu, Z.-Q. Zhao, Z.-P. Nie, and Q.-H. Liu, "The characteristics and affects of the microwave-induced thermo-acoustic signals in time and frequency domain," *Chinese of Journal Electronics*, Vol. 38, No. 3, 689–694, 2010.

18. Liu, Q. H., "The PSTD Algorithm: A time-domain method requiring only two cells per wavelength," *Microwave and Optical Technology Letters*, Vol. 15, No. 3, 158–165, 1997.